Available online at sjuoz.uoz.edu.krd

Science Journal of University of Zakho

Vol. 11, No. 4, pp. 515 – 522, October -December 2023

p-ISSN: 2663-628X
e-ISSN: 2663-6298

journals.uoz.edu.krd

DEVELOPING DURABLE SUPERAMPHIPHOBIC COATING ON ROUGH ALUMINUM USING RESIDUAL FROM BURNED RECYCLED SILICONE RUBBER FOR ANTI-CORROSION

Gulistan Taher Choli a*, Zubayda Shaheen Saifaldeenb

a Department of Physics, College of Science, University of Duhok. (gulistanphysics0@gmail.com)
b Scientific Research Center, College of Science, University of Duhok. (Zubayda.saifaldeen@uod.ac)

Received: 11 Aug., 2023 / Accepted: 16 Sep., 2023 / Published: 11 Nov., 2023. https://doi.org/10.25271/sjuoz.2023.11.4.1187

ABSTRACT:
This study presents a new, cost-effective, and environmentally friendly approach for creating a superamphiphobic coating. The method involves using a spray coating technique to apply silicone rubber onto smooth and micro-rough aluminum (Al) substrates. To enhance the coating's surface energy reduction, a thin layer of silicone rubber – trifluorotoluene (SR-TFT) was added. The morphology and chemistry of the coatings were analyzed utilizing scanning electron microscopy (SEM), energy dispersive X-ray spectroscopy (EDS), atomic force microscopy (AFM), and Fourier Transform Infrared Spectrometer (FTIR). The coatings displayed superamphiphobic properties with contact angles (CAs) of 170° for water and over 150° for both glycerol and ethylene glycol. Additionally, a remarkably low water droplet sliding angle (SA) of less than 2° was observed for surfaces coated with silicone rubber (SR)- trifluorotoluene (TFT), whether smooth or roughened. The coatings were tested for mechanical and chemical durability by impinging water droplets and immersing them in an acidic liquid respectively. The results showed that SR-TFT-coated silicone rubber on micro-rough Al substrates maintained its superamphiphobic property and exhibited excellent corrosion resistance compared to hydrophilic Al plates. Furthermore, the coatings displayed self-cleaning properties when water droplets were poured over a dusty surface, as the rolling water droplets effectively collected contaminant particles, leaving the surface of the sample clean. These findings indicate potential applications for the developed coatings as self-cleaning surfaces in challenging environmental conditions.
KEYWORDS: recycling silicone rubber, aluminum, mechanical sanding, superamphiphobicity, robustness.

1. INTRODUCTION

Superamphiphobic surfaces, combining superhydrophobic (SHP) and superoleophobic (SOP) properties, have gained significant attention due to their wide-ranging applications in antifouling, anti-icing, anti-corrosion, and oil-water separation*(J. Chen et al., 2019; Huang & Yu, 2021; Li et al., 2021; Liao & Zhu, 2021; Lv et al*., 2015; Saifaldeen *et al*., 2014; Steele *et al*., 2009; G. Wang *et al*., 2021; N. Wang & Xiong, 2014) Inspired by nature, such surfaces have been observed in lotus leaves with their water-repellent characteristics and marine species, which exhibit oil-repellent features (Xu *et al.*, 2016). The relationship between a solid material and a liquid substance is controlled by the solid's surface energy. Adjusting this connection has the potential to result in either hydrophobic or oleophobic characteristics. Roughness and changes in surface chemistry are common methods to achieve this tuning where low surface energy and increased surface area of interaction contribute to the desired properties. However, obtaining superoleophobic surfaces has been more challenging due to the need for robust re-entrant rough structures, which are often achieved using expensive techniques (J. Chen *et al.*, 2019; Saifaldeen *et al.*, 2014). Designing surfaces with superamphiphobic properties necessitates a thoughtful balance between the energy of the solid surface and the surface tension of the liquid. Superhydrophobic surfaces can be achieved through surface roughness, while superoleophobic surfaces demand additional strategies due to their low surface energy. Low liquid-solid contact fractions and surface energies are crucial for superoleophobicity, often achieved using surface complex with very low surface energy materials such as fluorinated compounds. Reentrant and doubly reentrant surface
structures are employed to enhance both water and oil repellency(J. Chen *et al.*, 2019; Huang & Yu, 2021; Steele e*t al.*, 2009; Liu & Kim, 2014).
Various technologies have been employed to fabricate superamphiphobic surfaces, including chemical etching, sol-gel processing, dip coating, laser ablation, spray coating, and spin coating (Steele et al., 2009; N. Wang & Xiong, 2014; Xu et al., 2016; Arianpour *et al.*, 2013; Barthwal *et al.*, 2013; Rico *et al.*, 2020). However, some of these methods suffer from high costs or produce chemical byproducts. Seeking sustainable and cost-effective solutions, polymers have emerged as promising materials for constructing superhydrophobic and superamphiphobic surfaces. For instance, silicone rubber treated with silica powder has been used to create superhydrophobic coatings, while ZnO nanoparticles mixed with a waterborne perfluoro acrylic polymer emulsion were employed for spray coating superamphiphobic surfaces (Li et al., 2021; Steele et al., 2009; F. J. Wang et al., 2013).
In this research, we introduce an innovative and environmentally friendly method for producing superamphiphobic coatings. The technique involves recycling silicone rubber, easily available in TV remote controllers, which is ultrasonicated in trifluorotoluene (TFT) solution and spray coated onto smooth and roughened aluminum (Al) metallic substrates. The simplicity and cost-effectiveness of these techniques offer promising potential for real-world applications of superamphiphobic coatings.

2. MATERIAL and METHODS

2.1. Film preparation

For the film preparation, commercially available Aluminum (Al) alloy 2024 was purchased from onlinemetals.com in America. The elemental composition, as determined by EDX, and the corresponding percentage ratios are displayed in Table [1]. The

* Corresponding author

metal was subsequently cut into small pieces measuring 1.5 cm × 2 cm to serve as substrates. These substrates underwent grinding using fine sandpapers of large grit sizes, specifically 3000 and 4000, to eliminate surface contaminants. Subsequently, the polished substrates were subjected to ultrasonication in acetone for 10 minutes. The silicon rubber found in TV remote controllers was recycled through a combustion process, resulting in a fine powder. This powder was then ultrasonicated in TFT, with a mixture of 20 mg of silicone rubber in 1 mL of TFT, for 1 hour to create a precursor solution of 7 ml. For the first set of samples, the precursor solution was spray-coated onto the smooth aluminum substrates. In contrast, for the second group of samples, the aluminum substrates were first roughened utilizing a variety of sandpapers with grit sizes of 60, 100, 220, and 400, and then coated with the produced precursor using the same spray coating method. This method entails maintaining a consistent 14 cm distance between the spray gun and the substrate, along with strict control of the aluminum substrate's temperature within a specific range of 90 ± 5°C. To ensure the stability of the substrate, a clamping device was employed to secure it above the heater at a height of 1 cm. It's worth noting that fluctuations in room temperature can have an impact on the duration of the spraying process. A schematic diagram illustrating the development of the two sets of coatings can be seen in Figure (1).

Table 1: Chemical Composition and Percentage Ratios of the Al 2024 Alloy Acquisition (Sunil Ratna Kumar, Ratnam, and Nagababu 2019).

Element	Percentage
Al	93.5
Cr	0.1 max
Cu	3.8 - 4.9
Mg	1.2 -1.8
Fe	0.5 max
Mn	0.3 - 0.9
Si	0.5 max
Zn	0.25 max
Ti	0.15 max

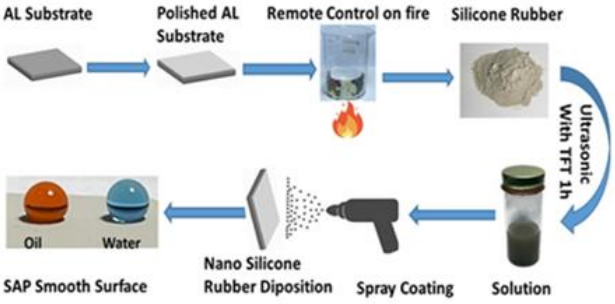

a. Nano Silicone Rubber Coating on Smooth Aluminum

Substrate.

b. Nano Silicone Rubber Coating on Micro-Rough Aluminum Substrate.

Figure 1: Schematic representation of the spray application procedure for Silicone Rubber onto (a) a smooth Aluminum base and (b) an Aluminum base with micro-rough structure.

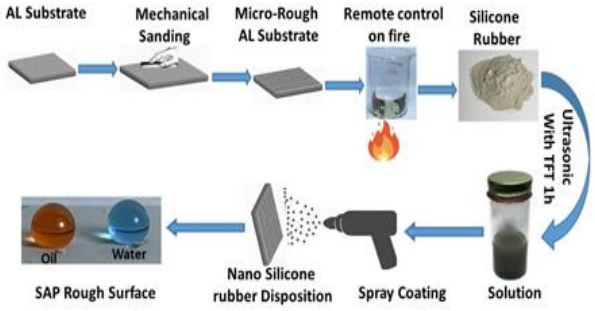

2.2. Characterizations

The surface structures of both groups of coatings were examined using Field Emission Scanning Electron Microscopy (FESEM, Zeiss-Gemini 560, Zeiss, Jena, Germany). Chemical characterization and elemental composition analysis of the coatings were conducted using an Energy-Dispersive X-ray (EDS) spectrometer (Zeiss, Jena, Germany) coupled with the FESEM device. Additionally, Fourier Transform Infrared Spectrometer (FTIR, Shimadzu 1800, Japan) methods were employed to analyze the chemical composition of the coatings. The wetting properties of both sets of coatings were determined by Calculating the contact angles (CAs) and sliding angles (SAs) of various liquid drops (approximately 2µL) using the sessile droplet technique and image J software (version 1.53a). The sliding angle (SAs) was measured by inclining the substrate until liquid droplets began to move off the surface. To ensure precision, five measurements were conducted for each sample, and subsequently, the average values for the contact angle and sliding angle were computed.

2.3. Robustness Analysis

The durability of the residual of burned recycled silicone rubber coatings exhibiting the greatest water resistance was evaluated by exposing them to water droplet impact from varying heights: 5 cm, 10 cm, 15 cm, and 20 cm. The procedure involved dropping 2.5 mL of water onto the same spot on the selected silicone rubber-coated surfaces from a height of 5 cm. Subsequently, the contact angles and sliding angles of the water droplets were measured at the impingement areas. The same procedure was repeated at heights of 10 cm, 15 cm, and 20 cm. To ensure accuracy, additional sets of spotless and rough clean samples, both before and after treatment, were used to average the presented data.

2.4. Corrosion Test

In order to evaluate the anti-corrosion properties of the newly developed superamphiphobic coatings, a solution containing sodium chloride (NaCl) at a concentration of 3.5% was created to mimic the environment found to seawater conditions. The corrosion test involved immersing the coatings in the prepared solution for different periods:24, 48, and 72 hours at room temperature. Subsequently, the samples were rinsed with deionized water and allowed them to air-dry at room temperature. The wetting characteristics were examined of the superamphiphobic surfaces and morphology was analyzed of the coatings after immersing in NaCl solution using Scanning Electron Microscopy (SEM) and Optical Microscopy (OM). The purpose of this analysis was to evaluate how the longevity of the coatings is influenced by exposure to harsh environment over an extended period.

2.5. Self-Cleaning test

To perform the auto-cleaning experiments, impurities in the form of carbon nanotube powder and soil powder were applied onto the surfaces of the developed coatings with the highest liquid-repellent properties. These coated samples were positioned on a

slightly slanted platform to facilitate the flow of water droplets across the surfaces. Then, water droplets were applied to the contaminated coatings in order to eliminate the impurities until the surfaces were cleansed. This procedure was repeated multiple times to ensure the reliability and precision of the results.

3. RESULTS AND DISCUDDION

3.1. The examination of surface structure and wetting properties

The aluminum substrate was mechanically roughed using various sandpaper grit sizes (60, 100, 220, 400, and 3000) to introduce micro-rough features. The size of micro features was substantially influenced by the sandpaper grit size and the direction of sanding also affected the form and size of the microstructures. SEM images (Figure 2a-e) demonstrated that increasing the sandpaper grit size results in a decrease in microstructure size and an increase in density. Each of these micro rough structures had a significant impact on the wetting characteristics, as observed by Saifaldeen *et al.* (2014) who created micro rough structures on aluminum alloy surfaces using various sandpaper grit sizes (36, 60, 120, 400, and 1000) through a simple scratching method. Investigating micro-nano rough Al substrates coated with silicone rubber (SR)-trifluorotoluene (TFT) using spray deposition for specific ratio coating, it was observed that decreasing the size of microstructures resulted in a reduction in the cavity of the double-layered rough surfaces due to a rise in the density and size of nanostructured silicone rubber nanoparticles(Figure 2f-j). The SEM analysis was used to characterize the surface structure of the silicone rubber coating applied to both smooth (Figure 2e, j) and rough AL substrates, utilizing various sandpaper grit sizes (60, 100, 220, and 400). Reducing the roughness of AL surfaces or the size of micro rough structures using larger sandpaper grit size caused a slight decrease in the cavity depth of the coating, and a more compact network. The SEM images showed that the agglomerated nanoparticles on all five coatings were completely covered by the spray coating, resulting in different double rough structures, as evident from the corresponding SEM images (Gong *et al*., 2020; Guo *et al*., 2020).

Much like the current study, previous research attempts have explored the utilization of silicone rubber materials. To the best of our knowledge, the closest work to the present study is Arianpour and colleagues (Arianpour *et al*., 2013) generated silicone rubber coatings by applying hexane-diluted solutions onto AL substrates using spin-coating techniques. Diverse amounts of carbon-black, Titania, or ceria nanopowders were incorporated into these coatings to modify their surface roughness and improve their superhydrophobic characteristics. In another research by Liao *et al.*(Liao & Zhu, 2021), a superhydrophobic coating was fabricated using vulcanized silicone rubber at room temperature combined with silica particles of different sizes. These materials were applied utilizing a layer-by-layer assembly technique on glass and copper foil substrates, resulting in a hierarchical structure of the micro-nano scale and rendering it highly water-resistant.

Elemental analysis of the prepared sample was conducted using FESEM-EDX to determine its elemental composition. The results depicted in Figure 3(a and b) indicated that the SR sample primarily comprised oxygen (O), silicon (Si), carbon (C), titanium (Ti), and sodium (Na). The reported weight percentages of these elements were as follows: silicone: 38.2wt%, O: 46.4wt%, C: 14.6wt%, Ti: 0.5wt%, and Na: 0.3wt%. These values represent the contamination rates of Ti (0.5wt%) and Na (0.3wt%)

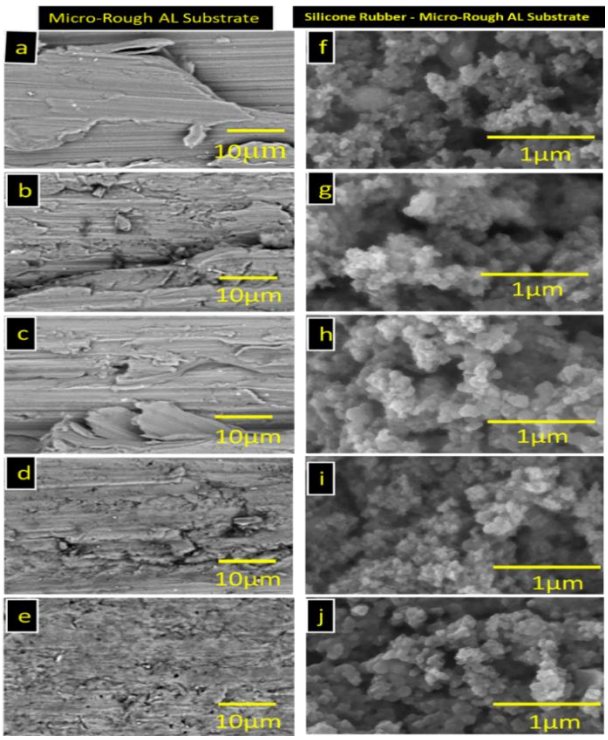

Figure 2: SEM images depict aluminum substrates with micro roughness (a-e), prepared using various sandpaper grit sizes (60, 100, 220, 400, and 3000). Top-view SEM images (f-j) show silicone rubber spray-coated on both smooth and micro-roughened aluminum substrates at a specific deposition ratio.

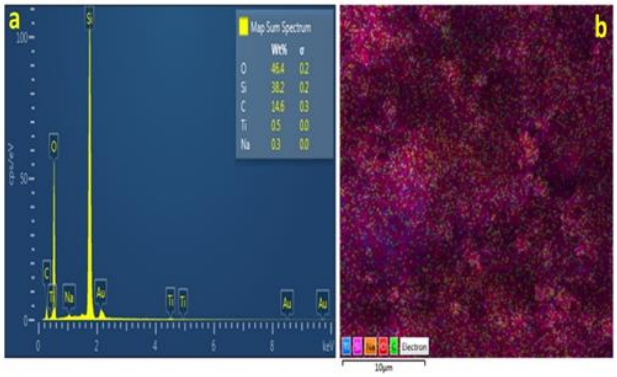

Figure 3: The FESEM-EDX mapping show: (a) the peaks corresponding to elements present in the sample, and (b) the layered EDX mapping demonstrate the distribution of the elements through the surface.

By utilizing a Fourier Transform Infrared Spectrometer (FTIR) and presenting the results in Figure (4), it becomes possible to determine the functional groups and chemical bonds present in both SR (silicone rubber) and SR-TFT (silicone rubber-trifluorotoluene) materials. The FTIR spectrum of silicone rubber exhibits several characteristic peaks, providing valuable information about its chemical composition. Notably, the most prominent peak observed at 1091 cm^{-1} is attributed to the asymmetric stretching vibration of the Si-O-Si bonds constituting the backbone of silicone rubber. Additionally, the appearance of a peak at 462.92 cm^{-1} signifies the existence of Si-OH bonds (Hu *et al*., 2018; Salih *et al*., 2018; Ye *et al*., 2017). Furthermore, the peak at 802.39 cm^{-1} is associated with methyl groups (-CH3) bonded to the silicon atoms, resulting from the symmetric stretching of Si-CH3 bonds (C. Chen *et al*., 2015; Hu *et al*., 2018; Salih *et al*., 2018). Moreover, the presence of carbonyl groups is designated by the peak at 1627.92 cm^{-1}, corresponding to the C=O stretching vibration, while the peaks at 2966.52 cm^{-1} and

3471.87 cm^{-1} correspond to the stretching oscillation of the C-H and O-H bonds, respectively (Cai *et al*., 2014; Ye *et al*., 2017).
In the FTIR spectrum of SR-TFT, slight changes in the wave number are observed which suggest the existence of comparable chemical bonds as found in silicone rubber. For instance, the peaks located at 470.63 cm^{-1} and 806.25 cm^{-1} are associated with Si-OH and Si-CH3 bonds respectively. Additionally, the tip at 1095.57 cm^{-1} represents the Si-O-Si stretching vibration. However, notable differences are observed when comparing SR-TFT to silicone rubber. In this case, a new chemical bond emerges, replacing a peak with a C=C characteristic at 1570.06 cm^{-1}. This shift indicates the formation of double bonds as a result of the interaction between Trifluorotoluene and silicone rubber. Interestingly, the peak at 2966.52 cm^{-1}, representing the C-H bond, remains consistent between the two materials. Furthermore, the peak at 3471.87 cm^{-1}, which corresponds to the O-H stretching vibration, is evident in both silicone rubber and silicone rubber-TFT. As a result, the existence of these shifts and the inclusion of the C=C bond within the SR-TFT spectrum result in a notable decrease in the surface energy of SR. This attribute can be further investigated by performing wetting assessments on the surface.

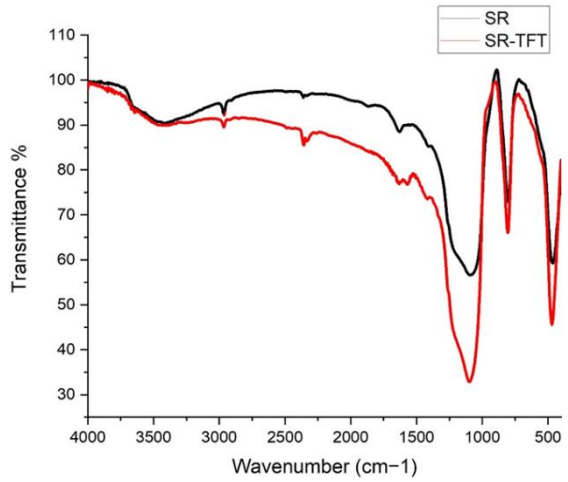

Figure 4:The FTIR of Silicone Rubber and Silicone Rubber-Trifluorotoluene.

The wetting analyses the two smooth and micro-rough aluminum substrates were created utilizing different sandpaper grit sizes of (60, 100, 200, 400, and 3000). For particular ratio deposition, these substrates were then coated with SR-TFT using the spray technique. The findings demonstrate that surfaces with a mix of microstructures coated with SR-TFT displayed superamphiphobic characteristics. Specifically, these surfaces had a (SA) of lower than 10° and a (CA) of over 150° for water, glycerol, and Ethelyn glycol. The use of sandpaper with a grit size of 60 gave the surface the biggest micro rough structures. This surface exhibited the highest CA values of 170°, 166.2°, and 162°, the lowest SA values of 0.5°, 2°, 9° for water, glycerol, and ethylene glycol respectively after being coated with silicone rubber-TFT. Additionally, the information in Figure 5(A, B, C) also demonstrates that the CAs of water, glycerol, and ethylene glycol droplets slightly decreased when the sandpaper grit size increased. When the rough surface was compared with the smooth surface that had been polished with the biggest grit size of 3000 sandpaper, it was observed that the smooth surface had a higher (SA) and a lower (CA) than the rough surface presented data in Figure 5. As a result, after optimization, Sandpaper grit size 60 has been selected as the ideal size. This means that the small grit sizes of the sandpaper used to make the microstructures on the Al layer are Profound adequate to support the Cassie state of wetting. In this state, liquid drops float on top of the air pockets inside the micro-nano structures. However, it was very hard to measure the (CAs) and (SAs) because the water drops barely touched the solid surface and quickly rolled away.

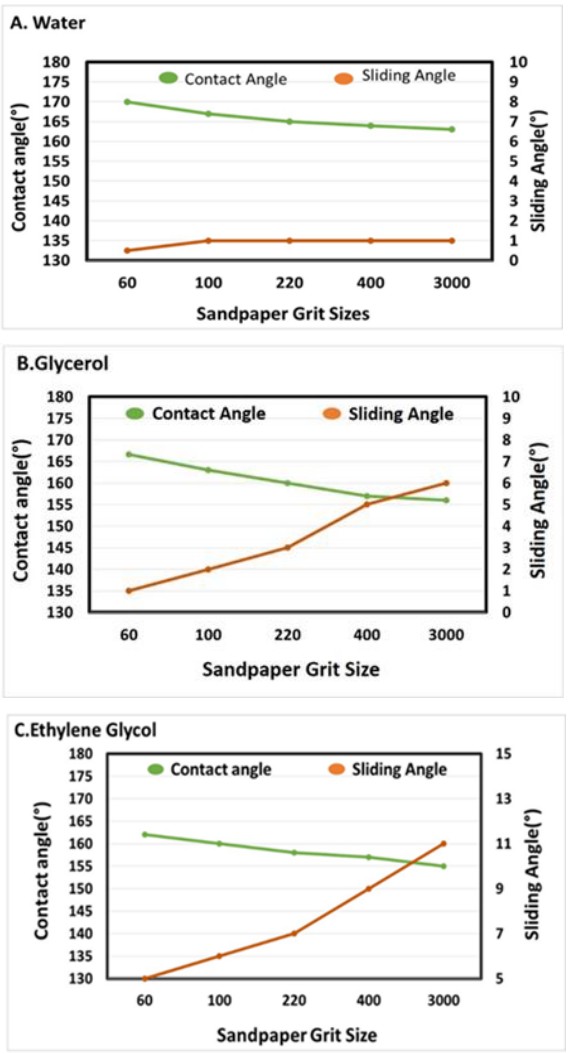

Figure 5:Contact angle and sliding angle were taken for 2 µL liquid drops on created surfaces via spray coating on micro-rough aluminum substrates with different sandpaper grit sizes, (a) water drops, (b) glycerol droplets, and (c) ethylene glycol droplets.

The wetting analyses were performed on the selected sample using different liquids with varying surface tensions. The sample consisted of a micro rough Al substrate created with 60 sandpaper grit size and coated with a silicone rubber-TFT solution (7ml). The investigation involved measuring the (CAs) of droplets for both water and some organic liquids. The coating displayed super repellency towards the water, which has a surface tension of approximately 72 mN/m, as well as moderately low surface tension liquids such as glycerol (GC) and Ethelyn glycol (EG) with surface tensions of approximately 63 and 47 mN/m, respectively. The surfaces with micro structures covered with silicone rubber-TFT showed superamphiphobic properties with (CAs) exceeding 150° and (SAs) lower than 10°
for water and oil. Hence, the surfaces that were prepared not only displayed superhydrophobic characteristics, but also showcased superoleophobic properties against liquids with relatively low surface tension. This outcome stemmed from the combination of low surface energy and the presence of dual micro-nano roughness.

The highest CAs of 170°, 166.7°, and 162° were observed for water, glycerol, and ethelynglycol respectively, after being spray-coated with silicone rubber-TFT, using sandpaper with a grit size of 60. The interaction of organic liquids, GC and EG, can also be explained by the Cassie model, as both liquids exhibited high CAs exceeding 150° and low SAs that were lower than 10 degrees, characteristic of the slippery Cassie state. However, the higher sliding angles and lower contact angles for the two organic liquids, compared to the very low sliding angle and contact angles for water, were attributed to higher CA hysteresis and more pinning of the contact line over the structures for the organic liquids. The study concluded that, as the surface tension of the liquid increases, the CA will also increase and vice versa; as shown in Figure 6.

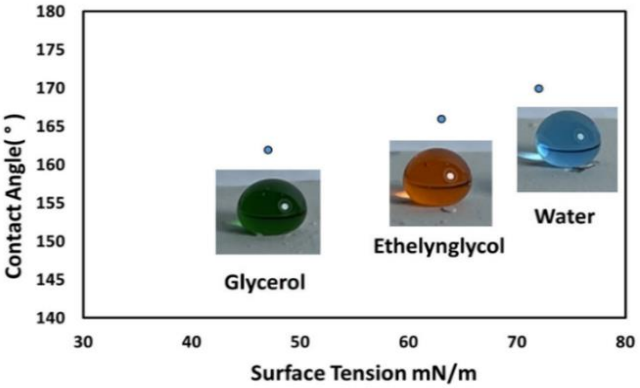

Figure 6: Shows contact angles of various liquids and their surface tension on the silicone rubber-TFT film, with accompanying photographic insets of the liquid droplets.

3.2. Observed contact angle analysis using basic wetting models.

To explain the findings of this study using fundamental wetting models, Figure 7 illustrates images of liquid droplets (water in blue, glycerol in orange, and ethylene glycol in green) on representative examples of the manufactured surfaces, including the bare or smooth AL alloy surface, submicron structured surface, and double structured surface.

For the bare or almost flat surface (Figure 7a), the smaller intrinsic contact angles of 29, 23, and 43 for glycerol, ethylene glycol, and water, respectively, align with Young's model. As specified by Young's model, the inherent contact angle of a liquid on a smooth solid surface is determined by the interfacial surface tensions associated with the interaction. A lower intrinsic contact angle is observed as the surface tension of the liquid decreases indicating reduced cohesion forces between its molecules. The AL alloy surface exhibits hydrophilic properties due to its intrinsic contact angles being less than 90 facilitating good wetting (S. & Lim, 2019; B. Zhang *et al*., 2020).

Moving to the submicro structured surface (Figure 7b), where a smooth AL substrate is coated with a nano network SR, the liquid droplets with different surface tensions have a spherical shape with contact angles higher than 150 degrees and sliding angles under 10°. These qualities can be assigned to the surface chemistry of the nanostructured surface, exhibiting superhydrophobic and superoleophobic features, consistent with the Wenzel model. SEM images indicate a smaller number of holes and less trapped air between the structure's parts.

In the case of micro-nano structures or double-layer roughness (Figure 7c), a nano network SR was coated on a microstructured AL substrate using sandpaper with 60-grit sizes, designed to sustain the Cassie state of wetting. In this state, water drops are hanged above the air pockets that are contained inside the micro-nano structures. However, as a result of the reduced contact area between the solid and the liquid, the water droplets rapidly rolled away, which made it impossible to accurately measure the contact angles (CAs) and slide angles (SAs). Nevertheless, the micro-nano structures demonstrated superhydrophobic and superoleophobic characteristics, with CAs exceeding 150° and SAs under 10° for liquids with different surface tensions, showcasing the strong Cassie state of wetting and the surface's superamphiphobic property (SAP) for high surface tension liquids such as water and low surface tension oils (S. & Lim, 2019).

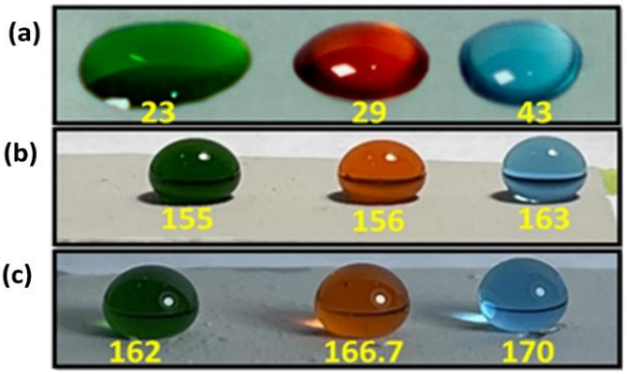

Figure 7: Photographic images were taken of distinct liquid drops including water (blue), glycerol (orange), and ethylene glycol (green), were evaluated on three types of surfaces: (a) a smoothly polished AL surface, (b) a nanostructured surface, and (c) a micro-nanostructured surface.

3.3. The Robustness Test

The robustness of the SHP (superhydrophobic) silicon rubber-TFT films was evaluated to investigate their long-term superhydrophobic characteristics, substrate adhesion, and durability. To perform the robustness test, water droplets of 2 microliters were continuously applied to the prepared samples from varying heights ranging from 5 cm to 20 cm. The objective of this experiment was to evaluate the surface's capacity to efficiently repel water and retain its superhydrophobic attributes without undergoing wetting.

The results showed that the SHP silicon rubber-TFT surface successfully exhibited the Lotus effect, a stable state of wetting known as the "slippery Cassie" state. This property is crucial for superhydrophobic surfaces used in applications such as auto-cleaning and anti-corrosion coatings. To ensure practical applicability, superhydrophobic surfaces must demonstrate strong adhesion properties and high mechanical stability.

In the durability assessment, surfaces demonstrating the most effective superhydrophobic qualities, identified by the highest contact angle (CA) and lowest sliding angle (SA), were selected from both the nanostructure and micro-nanostructure coatings. In the scenario of the silicone rubber-TFT coated nanostructured aluminum substrate (Figure 8), the contact angle (CA) values were measured both prior to and following the durability test. The findings revealed that the surface effectively maintained its superhydrophobic properties quite well at three different impact heights of 5 cm, 10 cm, and 15 cm—with a water contact angle exceeding 150 degrees. Nevertheless, the sliding angle saw an increase to over 10 degrees following the impact test. Upon raising the impact height to 20 cm, the surfaces lost their superhydrophobic nature. Even though they retained strong hydrophobicity, registering a water contact angle of 145, the upper layer of the silicone rubber-TFT coating was eradicated,

leading to an impact on surface adhesion and durability.

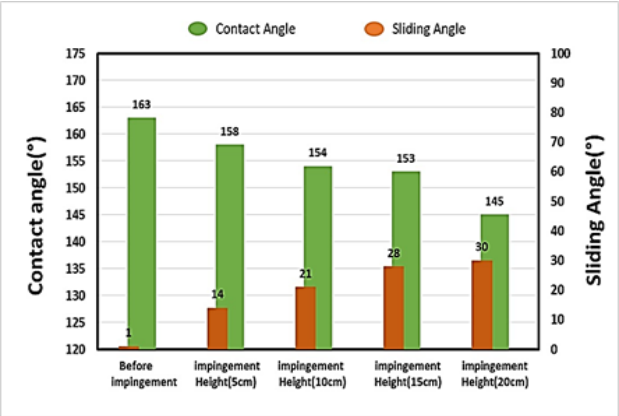

Figure 8. Investigation of the water interaction with the superhydrophobic silicone rubber-TFT coated on the smooth aluminum substrate with the best superhydrophobic qualities prior and after water drops impinged from four various heights of 5, 10, 15, and 20 cm; CA and SA measurements.

Liao *et al.* (Liao & Zhu, 2021) employed a layer-by-layer assembly technique to coat silicone rubber and silica particles of various sizes on glass and copper foil substrates, resulting in superhydrophobic properties and enhanced robustness and mechanical durability. Similar findings were presented by Long *et al.* (Long *et al*., 2017), who created superhydrophobic surfaces by spin-coating PDMS on a rough aluminum substrate, which improved surface roughness. In another study, Zhang *et al.* (B. Zhang *et al*., 2021) deposited a PDMS-CS double layer on a smooth aluminum substrate using scratch and direct coating methods, leading to superhydrophobic characteristics and increased robustness and durability compared to a pure CS-coated surface.

For the scenario involving dual-layer surface roughness, a micro-rough aluminum base was coated with SR-TFT utilizing the spray method. The surface effectively retained its superhydrophobic properties throughout and following the durability assessment. The contact angle (CA) values at impingements height of 5 cm, 10 cm, 15 cm, and 20 cm were presented in Figure 9 indicating that the surface remained continuously superhydrophobic with a water contact angle of over 150 degrees for all four impingement heights demonstrating its high resistance.

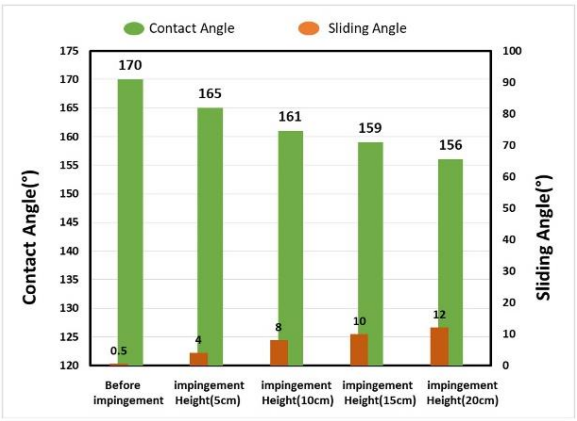

Figure 9: Wetting study of the micro-rough AL substrate coated silicone rubber-TFT with the best super-repellent qualities prior and after water drops impacted from four various heights of 5, 10, 15, and 20 cm; CA and SA measurements.

Through this investigation, it was found that double-layer roughness enhances superhydrophobicity and improves the adherence of the silicone rubber nano networks to the substrate(S. & Lim, 2019; Milles *et al.*, 2021). The increased surface area of the high surface energy aluminum substrate allows for a larger contact area with the low surface energy SR material. This improved adhesion results in a stronger and more compact material which is making it suitable for a wider range of applications due to its enhanced properties.

3.4. Corrosion Test

Corrosion resistance is a crucial property for metals and superamphiphobic coatings. The surface structures of corroded aluminum alloy 2024 samples in a 3.5% NaCl solution were analyzed using SEM and OMC images (Figure 10). As the time of immersion increased from 24 hours to 48 hours to 72 hours, the corrosion process became more intense in both smooth and rough AL substrates (Figure 10 a, b). The damaged surfaces displayed a porous structure, indicating the presence of pit corrosion, a localized form of corrosion that creates small holes or pits on the material's surface. After 72 hours, the micro-rough AL surface exhibited two types of corrosion: pits and cracks. Notably, corrosion was more pronounced on the rough aluminum surface compared to the smooth surface due to the presence of more cracks and exposed areas where the corrosive solution could penetrate, leading to increased corrosion.

Prakashaiah *et al.* (Prakashaiah *et al.*, 2018) conducted a study on the corrosion behavior of the 2024-T3 aluminum alloy in a 3.5% NaCl solution for 1 and 7 days, without inhibitors. They observed an increase in the corrosion process with longer exposure times, leading to a micro-porous structure on the corroded surface, indicating pit corrosion. Zhang et al.(X. Zhang *et al*., 2020) investigated the localized corrosion of AL alloy 2024 during submersion in a 3.5 wt.% NaCl solution for 2 hours and 15 hours. The corrosion process showed intergranular corrosion and crystallographic pitting, progressing sequentially from intergranular attack in the early stage to selective attack of the grain interior in the later stage.

In our investigation, we conducted corrosion testing on both smooth and rough superamphiphobic samples immersed in the same solution for a specific period. The SEM and OMC images showed minimal differences in surface morphologies for both samples under identical test conditions, before and after corrosion (Figure 10 c, d). This indicates that the SR coating provides corrosion protection, possibly through changes in the aluminum surface chemistry or the Attendance of a protective barrier layer. Moreover, the superamphiphobicity of the coated samples was well maintained, with a contact angle of more than 150 degrees for water and oil. However, with increased exposure time, the contact angle decreased (Liao & Zhu, 2021), as shown in Table 2. Lv *et al.* (Lv *et al.*, 2015) investigated the long-term corrosion resistance of hydrophilic AL and superhydrophobic surfaces on an aluminum base immersed in a 3.5 wt. % NaCl solution for 7 days. The hydrophilic aluminum sample displayed numerous cracks. In contrast, the superhydrophobic surface demonstrated only minor alterations and showcased impressive resistance to corrosion. However, it did experience a slight reduction in the contact angle and an increase in the sliding angle. Similarly, Wang *et al.* (N. Wang & Xiong, 2014) studied the corrosion resistance of a superhydrophobic surface on a steel substrate submerged in a 3.5 wt. % NaCl solution and discovered that the corrosion resistance primarily depends on the chemical composition, particularly the presence of extended hydrophobic chains, rather than solely on surface morphology.

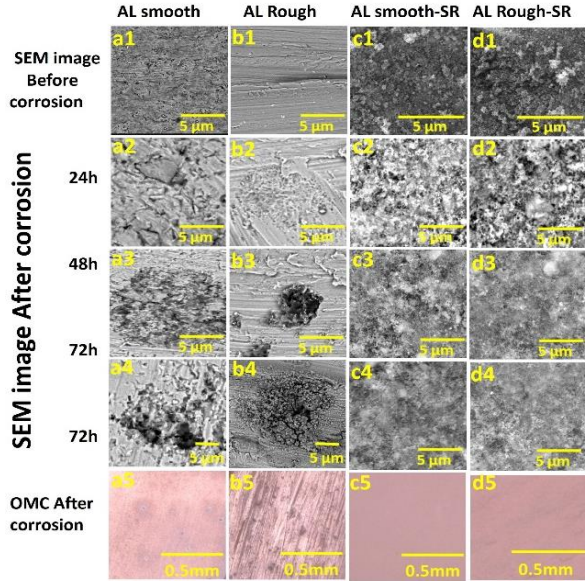

Figure 10: The SEM images of the samples prior and after corrosion in a 3.5% NaCl solution for 24 hours, 48 hours, and 72 hours are as follows: The hydrophilic AL smooth(a), the hydrophilic AL Rough(b), the superamphiphobic (AL smooth-SR) (c), and the superamphiphobic (AL Rough-SR). For a5,b5,c5, and d5 OMC images before 72h.

Table (2) Measurement of contact angle before and after corrosion.

samples			Water (CA)	Glycerol (CA)	Ethylene Glycol (CA)
Before corrosion	AL smooth-SR		163	156	155
	AL Rough-SR		170	166.7	162
After corrosion	AL smooth-SR	24h	159	155	153.5
		48h	156.2	154	152
		72h	154	152	151.2
	AL Rough-SR	24h	164	163	157
		48h	163.4	162.3	155
		72h	157	159	154.5

3.5 Self-cleaning Investigation

The ability to self-clean is a vital characteristic of super-repellent surfaces and the lotus leaf is a widely recognized example of a natural superhydrophobic surface known for its impressive self-cleaning capabilities. In this study, we experimented by evenly applying carbon nanotube (CNT) powder and soil powder onto a superhydrophobic silicone rubber surface (Figure 11). Droplets of water were then introduced onto the surface, and upon impact, they formed spherical droplets that rolled off the surface carrying dirt and waste with them and effectively keeping the surface clean. The test results demonstrated that the silicone rubber surfaces exhibited self-cleaning properties for both CNT and soil contaminants. Consequently, the surface can remain clean without the need for external cleaning methods.

The successful demonstration of self-cleaning properties in this experiment indicates that SR coatings can find applications in different industries such as aerospace, automotive, and construction, where maintaining clean surfaces is of great importance.

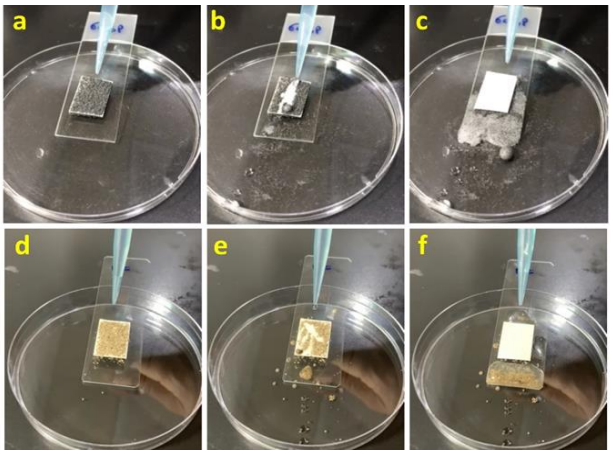

Figur 11: The auto-cleaning behavior of SR-TFT film utilizing(a-c) CNT powder (d-f) and soil powder as contamination.

4. CONCLUSIONS

In conclusion, we successfully developed robust superamphiphobic coatings on aluminum (AL) substrates using a simple spray-coating method. By coating residual from burned recycled silicone rubber with trifluorotoluene (SR-TFT) on the two smooth and micro-rough AL samples, we achieved coatings with excellent superamphiphobic properties. These coatings exhibited high contact angles (CAs) for water, glycerol, and ethylene glycol, also low sliding angles (SAs) for water drops on both smooth and rough metal surfaces.

Notably, the addition of the SR material on a micro-roughened AL substrate significantly enhanced both the superamphiphobic property and the robustness of the coatings. This improvement was achieved through the creation of a hierarchical roughness, combining micro-rough AL structures with a nanostructure of SR material. The synergistic effect of these characteristics played a crucial role in enhancing the coatings' repellency towards liquids and their mechanical strength.

Furthermore, the superamphiphobic surfaces demonstrated remarkable corrosion resistance when compared to hydrophilic AL surfaces. Additionally, the coatings displayed effective self-cleaning properties, making them highly promising for various applications.

Overall, this study highlights the potential of superamphiphobic coatings in diverse industries due to their outstanding repellent properties, mechanical durability, and corrosion resistance. These findings pave the way for future advancements and actual applications in aerospace, automotive, construction, and other fields where maintaining clean and robust surfaces is critical.

References

Arianpour, F., Farzaneh, M., & Kulinich, S. A. (2013). Hydrophobic and ice-retarding properties of doped silicone rubber coatings. *Applied Surface Science*, *265*, 546–552. https://doi.org/10.1016/j.apsusc.2012.11.042

Barthwal, S., Kim, Y. S., & Lim, S. H. (2013). Mechanically robust

superamphiphobic aluminum surface with nanopore-embedded microtexture. *Langmuir*, *29*(38), 11966–11974. https://doi.org/10.1021/la402600h

Cai, S., Zhang, Y., Zhang, H., Yan, H., Lv, H., & Jiang, B. (2014). *Sol − Gel Preparation of Hydrophobic Silica Antire fl ective Coatings with Low Refractive Index by Base / Acid Two-Step Catalysis*. 8–13.

Chen, C., Jia, Z., Wang, X., Lu, H., & Guan, Z. (2015). *Micro Characterization and Degradation Mechanism of Liquid Silicone Rubber Used for External Insulation*. *22*(1), 313–321. https://doi.org/10.1109/TDEI.2014.004188

Chen, J., Liu, Z., Wen, X., Xu, S., Wang, F., & Pi, P. (2019). Two-Step Approach for Fabrication of Durable Superamphiphobic Fabrics for Self-Cleaning, Antifouling, and On-Demand Oil/Water Separation. *Industrial and Engineering Chemistry Research*, *58*(14), 5490–5500. https://doi.org/10.1021/acs.iecr.9b00049

Gong, A., Zheng, Y., Yang, Z., Guo, X., Gao, Y., & Li, X. (2020). lW re of. *Materials Today Communications*, 101828. https://doi.org/10.1016/j.mtcomm.2020.101828

Guo, Y. (2020). & C corrosion Wetting and tribological properties of superhydrophobic aluminum surfaces with different water adhesion. *Journal of Materials Science*. https://doi.org/10.1007/s10853-020-04733-0

Hu, C., Chen, W., Li, T., Ding, Y., Yang, H., & Zhao, S. (2018). *Constructing non- fl uorinated porous superhydrophobic SiO 2 based fi lms with robust mechanical properties*. *551*(February), 65–73. https://doi.org/10.1016/j.colsurfa.2018.04.059

Huang, X., & Yu, R. (2021). Robust superhydrophobic and repellent coatings based on micro/nano SiO2 and fluorinated epoxy. *Coatings*, *11*(6). https://doi.org/10.3390/coatings11060663

K. Sunil Ratna Kumar, C. Ratnam, B. Nagababu, Fabrication and mechanical behavior of Al 2024-B4C MMCs and Al 2024- B4C -GR hybrid MMCS through powder metallurgy technique, Mater. Today Proc. 18 (2019) 219–229.

Li, A., Wang, G., Ma, Y., Zhao, C., Zhang, F., He, Q., & Zhang, Z. (2021). Study on preparation and properties of superhydrophobic surface of RTV silicone rubber. *Journal of Materials Research and Technology*, *11*, 135–143. https://doi.org/10.1016/j.jmrt.2020.12.074

Liao, K., & Zhu, J. (2021). A facile and cost-effective method to prepare a robust superhydrophobic RTV silicone coating. *Coatings*, *11*(3). https://doi.org/10.3390/coatings11030312

Liu, T., & Kim, C. J. (2014). Turning a surface superrepellent even to completely wetting liquids. *Science*, *346*(6213), 1096–1100. https://doi.org/10.1126/science.1254787

Long, M., Peng, S., Deng, W., Yang, X., Miao, K., Wen, N., Miao, X., & Deng, W. (2017). Robust and thermal-healing superhydrophobic surfaces by spin-coating of polydimethylsiloxane. *Journal of Colloid And Interface Science*. https://doi.org/10.1016/j.jcis.2017.08.027

Lv, D., Ou, J., Xue, M., & Wang, F. (2015). Stability and corrosion resistance of superhydrophobic surface on oxidized aluminum in NaCl aqueous solution. *Applied Surface Science*, *333*, 163–169. https://doi.org/10.1016/j.apsusc.2015.02.012

Milles, S., Dahms, J., & Soldera, M. (2021). *Stable Superhydrophobic Aluminum Surfaces Based on Laser-Fabricated Hierarchical Textures*.

Prakashaiah, B. G., Vinaya Kumara, D., Anup Pandith, A., Nityananda Shetty, A., & Amitha Rani, B. E. (2018). Corrosion inhibition of 2024-T3 aluminum alloy in 3.5% NaCl by thiosemicarbazone derivatives. *Corrosion Science*, *136*(March 2018), 326–338. https://doi.org/10.1016/j.corsci.2018.03.021

Rico, V., Mora, J., García, P., Agüero, A., Borrás, A., González-Elipe, A. R., & López-Santos, C. (2020). Robust anti-icing superhydrophobic aluminum alloy surfaces by grafting fluorocarbon molecular chains. *Applied Materials Today*, *21*. https://doi.org/10.1016/j.apmt.2020.100815

Salih, S. I., Oleiwi, J. K., & Ali, H. M. (2018, December). Study the Mechanical Properties of Polymeric Blends (SR/PMMA) Using for Maxillofacial Prosthesis Application. In IOP Conference Series: Materials Science and Engineering (Vol. 454, No. 1, p. 012086). IOP Publishing.

Sl, S. B. and, & Lim. (2019). No TitleRapid Fabrication of Dual-Scale Micro-nanostructured Superhydrophobic Aluminum Surface with Delayed Condensation and Ice Formation Properties. *Soft Matter*. doi: 10.1039/C9SM01256G.

Smaifaldeen, Z. S., Khedir, K. R., Cansizoglu, M. F., Demirkan, T., & Karabacak, T. (2014). Superamphiphobic aluminum alloy surfaces with micro and nanoscale hierarchical roughness produced by a simple and environmentally friendly technique. *Journal of Materials Science*, *49*(4), 1839–1853. https://doi.org/10.1007/s10853-013-7872-x

Steele, A., Bayer, I., & Loth, E. (2009). Inherently superoleophobic nanocomposite coatings by Spray Atomization. *Nano Letters*, *9*(1), 501–505. https://doi.org/10.1021/nl8037272

Wang, F. J., Lei, S., Ou, J. F., Xue, M. S., & Li, W. (2013). Superhydrophobic surfaces with excellent mechanical durability and easy repairability. *Applied Surface Science*, *276*, 397–400. https://doi.org/10.1016/j.apsusc.2013.03.104

Wang, G., Zhou, W., Zhou, J., Wang, M., Zhang, Y., & Qiang, H. (2021). Superhydrophobic silicone rubber surface prepared by direct replication. *Surface Engineering*, *37*(3), 278–287. https://doi.org/10.1080/02670844.2020.1776669

Wang, N., & Xiong, D. (2014). Superhydrophobic membranes on metal substrate and their corrosion protection in different corrosive media. *Applied Surface Science*, *305*, 603–608. https://doi.org/10.1016/j.apsusc.2014.03.142

Xu, C., Shi, Z., Wu, Z., & Zhang, F. (2016). *Fabrication of Superhydrophobic Soot-like Surface*. 400–403.

Ye, H., Zhu, L., Li, W., Liu, H., & Chen, H. (2017). *Constructing Fluorine-Free and Cost-E ff ective Superhydrophobic Surface with Normal-Alcohol-Modi fi ed Hydrophobic SiO 2 Nanoparticles*. https://doi.org/10.1021/acsami.6b12820

Zhang, B., Duan, J., Huang, Y., & Hou, B. (2021). Double layered superhydrophobic PDMS-Candle soot coating with durable corrosion resistance and thermal-mechanical robustness. *Journal of Materials Science and Technology*, *71*(April), 1–11. https://doi.org/10.1016/j.jmst.2020.09.011

Zhang, B., Zeng, Y., Wang, J., Sun, Y., Zhang, J., & Li, Y. (2020). Superamphiphobic aluminum alloy with low sliding angles and acid-alkali liquids repellency. *Materials & Design*, *188*(7), 108479. https://doi.org/10.1016/j.matdes.2020.108479

Zhang, X., Zhou, X., Hashimoto, T., & Liu, B. (2017). Localized corrosion in AA2024-T351 aluminium alloy: Transition from intergranular corrosion to crystallographic pitting. Materials Characterization, 130, 230-236.